IEEE Open Access Journal of Power and Energy

Received 22 March 2023; revised 12 July 2023; accepted 17 August 2023.
Date of publication 22 August 2023; date of current version 7 September 2023.

Digital Object Identifier 10.1109/OAJPE.2023.3307579

Performance Assessment of Flexible Links in Distribution Networks Using a Detailed Power Losses Model

FRANCISCO DE PAULA GARCÍA-LÓPEZ, MANUEL BARRAGÁN-VILLAREJO, ALEJANDRO MARANO-MARCOLINI (Member, IEEE), AND JOSÉ MARÍA MAZA-ORTEGA (Senior Member, IEEE)

Department of Electrical Engineering, Universidad de Sevilla, 41092 Seville, Spain

CORRESPONDING AUTHOR: F. d. P. GARCÍA-LÓPEZ (fdpgarcia@us.es)

This work was supported by Grant PID2021-124571OB-I00 funded by MCIN/AEI/ 10.13039/501100011033, by "ERDF A way of making Europe".

ABSTRACT The massive integration of distributed renewable energy resources is a reality in the current power system. In this new context with a greater volatility on the generation side it is required to incorporate new assets to provide additional flexibility to the system to accommodate as much renewable resources as possible. Among these new assets, DC or AC flexible links could play a key role in managing the power flows within radial distribution systems. These connected between distribution feeders may regulate the active power flow in a controlled manner and contribute to the network voltage support. However, the power losses of these devices can be a limiting factor of some functionalities. This paper integrates a detailed power loss model of several flexible link topologies for Optimal Power Flow algorithms with the aim of evaluating its impact on the functionalities of these devices. In this way, it is possible to benchmark the performance of different DC and AC flexible links in a quantitative manner by means of some key performance indexes. The paper proposes a case study based on the European MV benchmark with a high penetration of renewable energy sources to evidence the benefits and limitations that flexible links may provide.

INDEX TERMS Converter power losses, distributed renewable energy resources, flexible links, optimal power flow, vector switching converter, voltage source converters.

I. INTRODUCTION

GLOBAL energy consumption is still characterised by a high dependence on fossil primary energy [1], [2]. Fortunately, this trend is decreasing year by year thanks to the deployment of renewable energy generation, encouraged by most of the countries around the world. The International Renewable Energy Agency (IRENA) indicates that renewable energies have increased by 130% in the last decade (wind and photovoltaic energies 4 and 21 times respectively) with only 24% in non-renewable energies [3]. However, this report indicates that this increase is not yet sufficient to achieve the goal of reducing the earth's temperature by 1.5°C in 2030. In order to achieve this ambitous goal, 65% of the total energy produced should be from renewable sources for that year. In addition, IRENA proposes energy saving measures and efficiency improvements in the transmission and distribution networks to achieve a 4% reduction in power losses. With this future perspective, it is required to prepare the power system to accommodate as much renewable energy as possible in the most efficient way. This is a challenge considering the volatile nature of the renewable energy sources which will require a more flexible network operation. Therefore, the major investments on the grid should be displaced from conventional network assets, e.g. new transformers and/or lines, to new technologies which may bring the required additional flexibility.

The use of power electronics along with improved communication infrastructure, additional field measurements and advanced algorithms can facilitate the path towards an almost decarbonized power system. Within these power electronics based devices, flexible links (FLs) have emerged as a significant enabler for managing the power flows within distribution networks [4], [5]. A FL connects two or more radial feeders within a distribution network allowing a controlled power transfer between them as depicted in Fig. 1. These FLs can be classified based on the type of conversion used to interconect

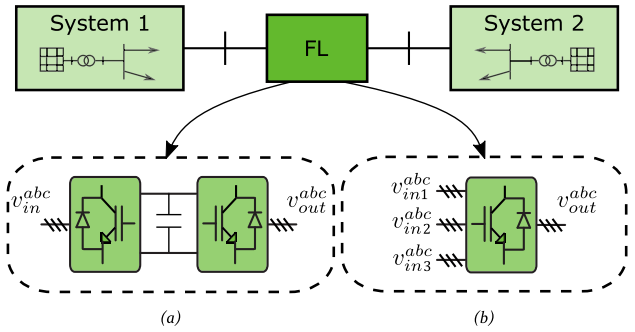

FIGURE 1. Single line diagram and three-phase diagram for two-level VSC and VeSC. (a) BTB or UPFC topologies. (b) VeSC topology.

the AC systems in DC or AC links. Typically, the power converters used for the DC links are Voltage Source Converters (VSCs) sharing a common DC bus, the most commonly used topologies for these links are Back to Back (BTB) and Unified Power Flow Controller (UPFC). On the contrary, AC links [7] directly performs the interconnection of the radial systems without using any DC intermediate bus. Vector Switching Converters (VeSCs) [6] are one of the most popular power converters used in case of AC links due to the reduced number of semiconductors and simple modulation strategies compared to traditional matrix converters. The topology used for AC links is AC-link shunt-series power flow controller (AC-link ShSPFC).

FL models can be found in the literature covering dynamic [8], [9] and steady-state conditions [10], [11]. The latter ones are of special interest for addressing the benefits that FLs may bring to the distribution network for reducing network losses [12], [13], voltage regulation [14], load balancing of power lines or transformers [15], maximization of the network loadability [4] or maximization of RES penetration [16]. In any of these applications, the FL converter power losses are key to evaluate the actual performance, especially in those cases where the FL functionality is related to the reduction of the overall system power losses.

The VSC power losses have been traditionally modeled in a simplified manner by a quadratic function depending on the VSC current and grouping the conduction and switching power losses [17]. The quadratic function terms are considered constant [18], [19] or variable but solely depending on the VSC current [20]. These models, although widely used in the literature, consider that the conduction losses only depend on the VSC current without taking into account other important VSC variables such as modulating index and power factor. With respect to the switching losses, a linear model of the VSC current and DC voltage is usually considered. This approximation helps to simplify the computation of switching losses but does not reflect the quadratic or even cubic dependency of these losses according to the manufacturers' datasheet. Some advanced models have detected this gap and propose separated models for the conduction and switching losses by means of two quadratic functions [21]. However, this proposal still does not take into account how the VSC power factor and the modulating signal affect the VSC power losses. Therefore, to the best knowledge of the authors, there is a lack of accuracy in the model of the VSC power losses required for the performance assessment of FLs in distribution networks.

On the contrary, and regarding the modelling of VeSC losses, Mancilla et al. presented in [22] a detailed VeSC power loss model depending on the VeSC output current and voltage, the duty ratio and manufacturer data (IGBT and diode datasheets).

This work proposes the use of different DC-link and AC-link topologies in distribution networks to improve the performance in case of a massive integration of Renewable Energy Sources (RES). The main objective of the paper is to compare the performance of the selected topologies in a quantitative manner and evidence the importance of modelling the FL power losses properly. Therefore, the main contributions of the paper can be summarized as follows:

- Detailed power loss model of VSCs and VeSCs taking into account the injected current, the modulation signal, the power factor and IGBT-diode datasheets.
- Integration of these power losses model within the Optimal Power Flow (OPF) algorithms used for computing the FL setpoints. With this regard, it is considered the topology in terms of number of VSCs/VeSCs and their interconnection to the distribution network.
- Quantitative performance comparison of different DC-link and AC-link topologies for meshing distribution networks with a high RES penetration.

The paper is organised as follows. Section II presents the most prominent FL topologies used in distribution networks. Section III describes the OPF formulation including FLs with their corresponding power loss model. Section IV evaluates the performace of the FL topologies in a benchmark distribution network with high RES penetration. For this purpose, the FL setpoints are computed by an OPF aimed at reducing the overall system power losses. The performance of the different FL topologies are compared in a quantitative manner by means of some Key Performance Indices (KPIs). Finally, Section V closes with the main conclusions and future research lines.

II. FLEXIBLE LINK TOPOLOGIES

This work analyzes three different flexible link topologies based either on VSCs or VeSCs. The main characteristics of each topology are briefly described in the following:

- Back-to-back VSC (BTB). This topology is made up of two VSCs sharing a common DC link, as shown in the one-line diagram of Fig. 2.a. Both VSCs are rated to withstand the network voltage and the current flowing between the interconnected feeders. Generally, the VSCs are connected to the network through a step-up transformer, but it also possible to use

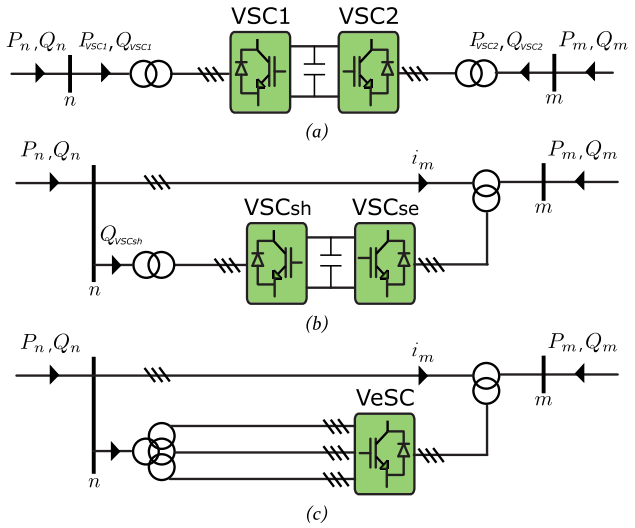

FIGURE 2. Single line diagram of the FL topologies. a) BTB, b) UPFC, c) AC-link ShSPFC.

transformerless configurations in case of using multilevel topologies [23]. In this configuration, one of the VSCs sets the active and reactive power injections while the other one controls the DC bus voltage and injects also reactive power. Therefore, this configuration allows an independent control of the active power flow between the interconnected feeders, P_m, and two reactive power injections at the corresponding Point of Interconnection (POI) of each VSC, Q_m and Q_n.

- Unified power flow controller (UPFC). This topology is composed of shunt- and series-connected VSCs, VSCsh and VSCse respectively, sharing a common DC bus as shown in Fig. 2.b. Like in the BTB case, this FL has three degrees of freedom (P_m, Q_m and Q_n.), being the VSCsh in charge of controlling the DC bus voltage. This topology, however, may force similar power flows in the network with a lower power rating. Particularly, note that the VSCse rated voltage is just a fraction of the rated network voltage leading to a reduced VSCse rated power. On the other hand, the VSCsh rated rated current mostly depends on the sum of the injected reactive powers $Q_m + Q_n$ as shown in Fig. 2.b. Therefore, the VSCsh rated power is directly related to the FL reactive power capability being possible to define three different operation modes [9]:
  - UPFC-P2Q. The VSCsh has the capacity to inject/absorb the reactive power of both interconnected feeders, i.e. $Q_m + Q_n \leq 2$ p.u.
  - UPFC-P1Q. The VSCsh reactive power capability is constrained to inject/absorb just the reactive power of one feeder, i.e. $Q_m + Q_n \leq 1$ p.u.
  - UPFC-P0Q. The VSCsh has no capability to provide reactive power, i.e. $Q_m + Q_n = 0$ p.u. Therefore, in this case the UPFC has just two degrees of freedom: P_m and Q_m.
- AC-link shunt-series power flow controller (AC-link ShSPFC). In this case, the shunt-series connection has been applied in a similar way as in the UPFC case as shown in Fig. 2.c [24]. This topology has just two degrees of freedom, P_m and Q_m, which are adjusted depending on the VeSC series voltage. This series voltage is synthesized from the combination of certain input voltages which are obtained from a multi-winding shunt transformer [6]. Regarding the rating of the AC link ShSPFC, it has the same advantages as the UPFC topology because the VeSC series voltage is just a fraction of the network voltage. Therefore, the rated power of the AC-link ShSPFC is a small part of the power transferred between the feeders.

III. OPF FORMULATION AND FL POWER LOSSES MODELLING

This section presents the general OPF formulation used to assess the ability of the different FLs to improve the distribution network operation and also the details of the power loss model of each FL topology.

A. STRUCTURE OF THE OPF

A general OPF aims to minimize or maximize a certain performance index, z, expressed as a function f which depends on the state, x, and control variables, u. State variables are the voltage magnitudes and angles of every busbar. Control variables are the active and reactive power injections at each FL terminal, $P_{m,n}$ and $Q_{m,n}$. Mathematicaly, the objective of the OPF can be stated as follows:

$$\min \quad z = f(x, u) \tag{1}$$

This optimization problem is subject to the equality constraints impossed by the active and reactive power balance for each bus:

$$P_i^{bal} = V_i \sum_j \left(V_j G_{ij} \cos\theta_{ij} + V_j B_{ij} \sin\theta_{ij}\right), \ \forall i \in \mathcal{N} \tag{2}$$

$$Q_i^{bal} = V_i \sum_j \left(V_j G_{ij} \sin\theta_{ij} - V_j B_{ij} \cos\theta_{ij}\right), \ \forall i \in \mathcal{N} \tag{3}$$

$$P_i^{bal} = P_i^{inj} - P_i^{abs}, \quad \forall i \in \mathcal{N} \setminus \{m, n\} \tag{4}$$

$$Q_i^{bal} = Q_i^{inj} - Q_i^{abs}, \quad \forall i \in \mathcal{N} \setminus \{m, n\} \tag{5}$$

$$P_k^{bal} = P_k^{inj} - P_k^{abs} - P_k, \quad k = \{m, n\} \tag{6}$$

$$Q_k^{bal} = Q_k^{inj} - Q_k^{abs} - Q_k, \quad k = \{m, n\}, \tag{7}$$

and the active power balance in the FL:

$$P_{loss}^{FL} + P_m + P_n = 0. \tag{8}$$

$\mathcal{N}$ is the set of buses; $P_i^{inj} + jQ_i^{inj}$ is the complex power injected by dispersed generators connected at bus i; $P_i^{abs} + jQ_i^{abs}$ is the complex load demanded at bus i; P_i^{bal} and Q_i^{bal} are the active and reactive power balances on bus i; $G_{ij} + jB_{ij}$ is the ij-element of the bus admittance matrix, which includes the admittances of the lines and of the converter coupling

filters; m and n are the FL connection buses; P_{loss}^{FL} are the FL internal power losses which is analyzed in the next subsection. Note that DC link losses are not taken into account. This is because the FLs are designed to be installed in switching centres where the distance between the DC buses of the VSCs is very short. Therefore, the losses of this part are not significant and can be neglected compared to the losses of the converters themselves.

The control variables $P_{m,n}$ and $Q_{m,n}$ depend on internal FL magnitudes, voltage and current, which are particularized for each topology. Thus, equations for the UPFC topologies (P2Q, P1Q and P0Q) can be found in [25] while those for the AC-link ShSPFC are detailed in [26].

Finally, this optimization problem is completed with some inequality constraints taken into account some operational limits of the network and FL:

$$0 \leq I_b \leq I_b^{max}, \quad \forall b \in \mathcal{B} \tag{9}$$

$$V_i^{min} \leq V_i \leq V_i^{max}, \quad \forall i \in \mathcal{N} \tag{10}$$

$$0 \leq S_{FL} \leq S_{FL}^{rat}, \tag{11}$$

where $\mathcal{B}$ is the set of branches, (9) is the conductor ampacity limit, (10) defines the bus voltage magnitude limits and (11) refers to the FL rated power limit.

B. VSC POWER LOSS MODEL

The power losses of a VSC correspond to the conduction and switching losses of IGBTs and diodes. The IGBT and diode average conduction power losses during the switching period, P_{cond}^{IGBT} and P_{cond}^{diode} respectively, are computed as follows [17], [27]:

$$P_{cond}^{IGBT} = I_o \cdot v_{ceo} \cdot \left(\frac{1}{2\pi} + \frac{y}{8}\right) + r_c \cdot I_o^2 \cdot \left(\frac{1}{8} + \frac{y}{3\pi}\right), \tag{12}$$

$$P_{cond}^{diode} = I_o \cdot v_{fo} \cdot \left(\frac{1}{2\pi} - \frac{y}{8}\right) + r_d \cdot I_o^2 \cdot \left(\frac{1}{8} - \frac{y}{3\pi}\right), \tag{13}$$

where $y = m \cdot \cos\phi$, v_{ceo} is the IGBT zero-current collector-emitter voltage, v_{fo} is the diode forward voltage, r_c and r_d are the IGBT and diode on-state resistance respectively, m is the peak value of the PWM modulating signal, $\cos\phi$ is the VSC power factor and I_o is the peak value of the output AC current. Parameters v_{ceo}, v_{do}, r_c and r_d are provided in the semiconductor datasheet and m, $\cos\phi$ and I_o depend on the VSC operating point.

On the other hand, the IGBT and diode switching power losses, P_{sw}^{IGBT} and P_{sw}^{diode}, are formulated as [27]:

$$P_{sw}^{IGBT} = \left(E_{on} + E_{off}\right) \cdot f_{sw}, \tag{14}$$

$$P_{sw}^{diode} = E_{rr} \cdot f_{sw}, \tag{15}$$

where E_{on} and E_{off} are the turn-on and turn-off energy losses of the IGBT, E_{rr} is the diode turn-off energy due to the reverse-recovery current, and f_{sw} is the switching frequency. These energy losses can be evaluated from the energy-current curves within the semiconductor datasheet through a least-squares fitting. In this way, the power losses can be formulated as a function of the AC output current as follows:

$$E_r = a_r \cdot I_{dc}^2 + b_r \cdot I_{dc} + c_r \;\; ; \;\; r = \{on, off, rr\} \tag{16}$$

where a_r, b_r and c_r are the parameters of the least squares fitting function for each energy-current curve and, I_{dc} is an equivalent DC output current through the IGBT/diode module on a half cycle of the output frequency [27] with $I_{dc} = I_o/\pi$.

Therefore, the total power losses of an IGBT-diode module is as follows:

$$P_{loss}^{module} = P_{cond}^{IGBT} + P_{cond}^{diode} + P_{sw}^{IGBT} + P_{sw}^{diode}, \tag{17}$$

and those corresponding to a VSC composed of k IGBT-diode modules are:

$$P_{loss}^{VSC} = k \cdot P_{loss}^{module} \tag{18}$$

C. VeSC POWER LOSSES MODEL

The VeSC power losses can be divided into conduction and switching losses which are formulated for each VeSC branch b as [22] (see (19) and (20), as shown at the bottom of the page), where f is the fundamental frequency, $q = f_{sw}/f$, V_{rms} and I_{rms} are the RMS VeSC output voltage and current and d_b is the duty ratio of the branch b. The rest of the parameters corresponds to the IGBT and diode characteristics which can be found in the manufacturer datasheet: v_{on} and i_{on} are the IGBT turn-on collector-emitter voltage and current, v_{off} and i_{off} are the IGBT turn-off collector-emitter voltage and current, v_{rr} and i_{rr} are the diode recovery voltage and current and E_{on}^{rat}, E_{off}^{rat} and E_{rr}^{rat} are the IGBT and diode switching energy losses. The total power losses of the VeSC depend on its number of branches as described in (21), as shown at the bottom of the page.

$$P_{cond}^{VeSC_b} = 3 \cdot d_b \cdot I_{rms,b} \cdot \left[\frac{\sqrt{2}}{\pi}\left(v_{ceo} + v_{fo}\right) + \frac{d_b \cdot I_{rms,b}}{2 \cdot 3}\left(r_c + r_d\right)\right] \tag{19}$$

$$P_{sw}^{VeSC_b} = 3 \cdot f \frac{V_{rms,b} I_{rms,b}}{d_b} \cdot \left[\sqrt{3}q + 9\frac{\cos\frac{d_b 2\pi}{q}\cos\frac{(1-d_b)2\pi}{q}}{\sin\frac{2\pi}{q}}\right] \cdot \left[\frac{E_{on}^{rat}}{v_{on} i_{on}} + \frac{E_{off}^{rat}}{v_{off} i_{off}} + \frac{E_{rr}^{rat}}{v_{rr} i_{rr}}\right] \tag{20}$$

$$P_{loss}^{VeSC} = \sum\nolimits_b \left(P_{cond}^{VeSC_b} + P_{sw}^{VeSC_b}\right) \tag{21}$$

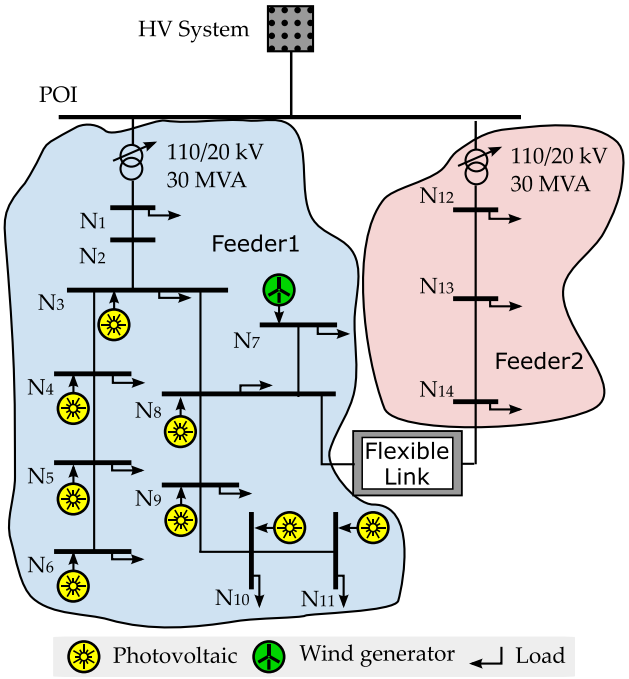

FIGURE 3. One-line diagram of the benchmark distribution system for evaluating the performance of the FLs.

IV. CASE STUDY

A. BENCHMARK DISTRIBUTION SYSTEM AND SCENARIO DEFINITION

The previously presented FL topologies have been tested in the MV distribution network defined by the CIGRE Task Force C06.04.02 [28] with the one-line diagram shown in Fig. 3. This distribution network is composed of two main feeders. Feeder 1, with a total line length of 15 km, has a mesh topology, but it is operated in a radial manner due to the use of normally open switches. Feeder 2 has a total line length of 8 km. Each feeder is connected to a primary substation through a 30 MVA 110/20 kV transformer. The network comprises 14 nodes, 11 of which are within Feeder 1. All network data including topology, line and cable parameters, loads, distributed RES and their corresponding daily load/generation curves are available in [28].

This network includes a BTB between nodes N14 and N8 with a total power of 6 MVA (two 3 MVA converters) [29]. Taking this device as a reference, the rating power of the rest of FLs is defined according to the characteristics described in Section II. Table 1 collects the rated magnitudes of the FL topologies under study. The impedance of the coupling filters is selected to 0.1 pu according to the rated voltage and power of each converter, with a quality factor (X/R) equal to 100.

Both VSCs and VeSCs have been assumed to be based on the same power electronics switch, namely the SKM1000GB17R8 provided by SEMIKRON [30]. Appendix V contains all the data required for the FL power loss model and the corresponding parameters used in (16).

TABLE 1. Rated magnitudes of the FLs. V_{rated} is the rated voltage of the converter, S_{rated} is the rated power of the converter and coupling transformer, and r_t is the transformer ratio.

FL	Converter	V_{rated} (V)	S_{rated} (MVA)	r_t (kV/kV)
BTB	VSC_1	400	3	20/0.4
	VSC_2	400	3	20/0.4
P0Q	VSC_{sh}	400	0.6	20/0.4
	VSC_{se}	200	0.6	0.2/0.2
P1Q	VSC_{sh}	400	3	20/0.4
	VSC_{se}	200	0.6	0.2/0.2
P2Q	VSC_{sh}	400	6	20/0.4
	VSC_{se}	200	0.6	0.2/0.2
ShSPFC	$VeSC$	200	0.6	0.2/0.2

In order to create a scenario with a massive RES integration, the original PV and wind generation included in [28] has been multiplied by 60 and 4 respectively. In this manner, the network has a 50% of RES penetration, i.e. RES peak power over peak demand, which is reasonable considering the current trend.

The FL setpoints for each time period t have been calculated by applying the OPF (1)-(11), particularizing the objective function to minimize the system total power losses:

$$z(t) = \sum_{\forall b \in \mathcal{B}} 3 \cdot I_b(t)^2 \cdot R_b + P^{FL}_{loss}(t). \tag{22}$$

where $I_b(t)$ is the current that circulates through the lines of the study system and R_b is the resistance value of the lines.

B. DEFINITION OF KPIs

This section is devoted to define some KPIs required to perform a quantitative comparison of the FL topologies. These KPIs are established with the aim of assessing and comparing the performance of each device in relation to the OPF objective and relevant operation variables.

- System energy losses, E_{loss} (MWh), which can be further divided into FL energy losses, E^{FL}_{loss}, and network energy losses, E^{net}_{loss}:

$$E_{loss} = D \sum_{\forall t \in \mathcal{T}} \left(\sum_{\forall b \in \mathcal{B}} 3 I_b(t)^2 R_b + P^{FL}_{loss}(t) \right), \tag{23}$$

  where $\mathcal{T}$ is the set of time periods t of duration D in which the day is discretized.
- Reduction in energy losses with respect to the base case (BC) without any FL (%):

$$\Delta E_{loss} = \frac{E^{BC}_{loss} - E_{loss}}{E^{BC}_{loss}} \cdot 100 \tag{24}$$

- Ratio between FL and system energy losses (%):

$$R_{FL-syst} = \frac{E^{FL}_{loss}}{E_{loss}} \cdot 100 \tag{25}$$

- Ratio between FL reactive energy and apparent energy (%):

$$R_Q(\%) = \frac{E_Q^{FL}}{E_S^{FL}} \cdot 100, \tag{26}$$

where the apparent energy managed by the FL is computed as: $E_S^{FL} = D \sum_{\forall t \in \mathcal{T}} (S_{N8}(t) + S_{N14}(t))\cdot$.

- Ratio between the FL maximum apparent power and FL rated power (%):

$$R_S(\%) = \frac{S_{max}^{FL}}{S_{rated}^{FL}}, \tag{27}$$

where S_{rated}^{FL} is the sum of the rated powers of the converters within the FL.

- Average feeder voltage (pu):

$$V_k = \frac{1}{|\mathcal{T}| \cdot |\mathcal{N}^k|} \sum_{\forall t \in \mathcal{T}} \sum_{\forall i \in \mathcal{N}^k} V_i(t) \tag{28}$$

where $|\cdot|$ refers to the cardinality of a set and $\mathcal{N}^k$ is the set of buses within feeder k.

Notice that KPIs (23) and (24) quantify system losses (the OPF main objective), KPI (25) discriminates the influence of the device's own losses versus system losses. KPIs (26) and (27) were established to compare the performance of the different topologies, assessing the performance of each one in relation to its nominal power, and the influence of reactive power injections. Finally, KPI (28) has been included to check, for each device, the effect on system voltages.

C. SIMULATION RESULTS AND DISCUSSION

This section presents the main results of the case study to evidence the benefits that FL may bring to distribution networks with a high RES penetration.

The OPF was modelled in GAMS and solved using the nonlinear solver Conopt [31].

First, the upper plot of Fig. 4 shows the 24-hour evolution of the system power losses for different FL topologies. A significant reduction of power losses with respect to the BC is achieved in all the cases, especially for those topologies with series converter, i.e. UPFC (P0Q, P1Q y P2Q) and AC-link ShSPFC. The figure reveals that the greatest reduction occurs around noon when PV generation is peaking. In this period, the FL transfer active power from feeder 1, where the PV generation is installed, to feeder 2. In this manner the total load is shared between the meshed feeders which leads to minimal power losses scenario. It is also interesting to note that during the rest of the day the system power losses for different FL topologies are also lower than in the BC except for the BTB and UPFC-P2Q cases. This is because these two FL topologies require large VSCs which have high power losses even in case of low load. This emphasizes the importance of considering an adequate FL power loss model when calculating the its setpoints by an OPF tool.

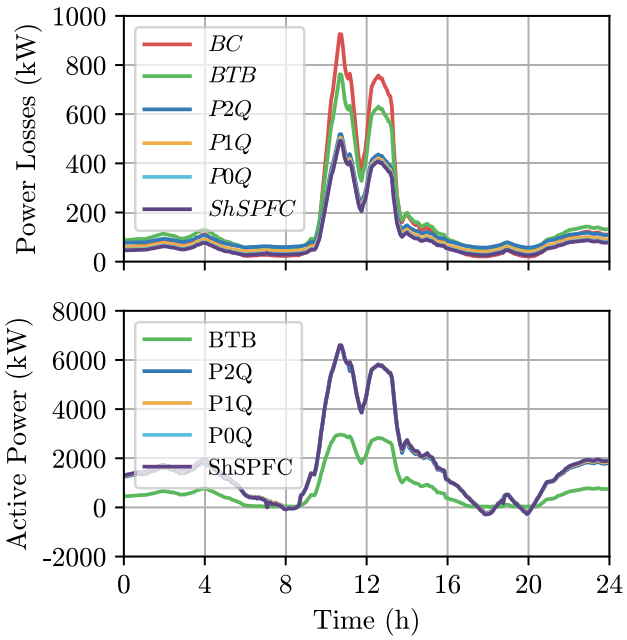

FIGURE 4. Upper plot: Daily evolution of system power losses for different FL topologies. Bottom plot: Active power absorbed by different FL topologies from bus N8.

The active power transfer from bus N8 to bus N14 is shown in the bottom plot of Fig. 4. Note that the BTB topology reaches its rated power, 3 MVA, around noon, which clearly limits the power transfer between the feeders, thus, the reduction of power losses as shown in the top plot of Fig. 4. On the contrary, the remaining topologies, which perform almost equally, have a higher active power transfer capacity thanks to the series injected voltage. In these cases, the power transfer is limited by the ampacity of the interconnected feeders remaining the series converters always below their rated voltage. Regarding the rest of the day, it is noteworthy that the power transferred by the BTB topology is null during large periods, revealing the importance of its own losses with respect to the network losses. At the end, the reduction of network power losses achieved by the power transfer between the feeders is surpassed with the increase of BTB power losses. It has to be considered that the FL has some power losses, even in the case of null power transfer, which justify the power losses increase with respect to the BC in this periods of the day.

The FL power losses are represented in the upper graph of Fig. 5, plotted on two ordinate axes due to the higher power losess of the BTB topology with respect the other ones since all the power transferred between the feeders goes through the power converters. The BTB power losses resembles the active power transfer between the feeders shown in Fig. 4 due to its cascade topology. Regarding the UPFC-P2Q topology, it has the second highest power losses due to the large shunt converter, which is rated to provide the reactive power of both interconnected feeders as depicted in Table 1. The reduction of the shunt converter sizing leads to lower power losses as can be noticed for the UPFC-P1Q topology. In any case, it is

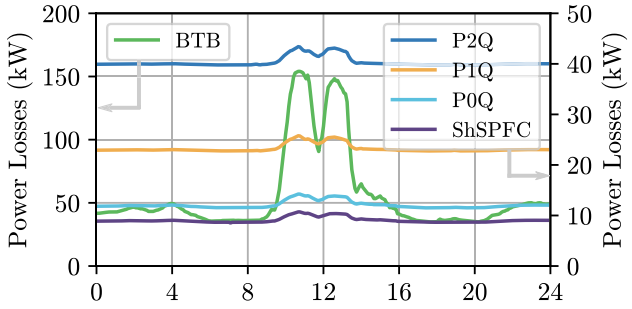

FIGURE 5. **Active power losses of the converters in each FL.**

important to highlight the impact that the FL power losses have in the optimal setpoints computed by the OPF. Note that the contribution of the series converter to the power losses of the UPFC-P2Q and UPFC-P1Q is almost negligible, since its apparent power is relatively small, as shown in Table 1. Finally, the AC-link ShSPFC has the lowest power losses since it consists of a single series-connected converter with low-rated power compared to the power transferred between feeders. It should be mentioned that the UPFC-P0Q has slightly higher active power losses than the AC-link ShSPFC due to the higher number of IGBTs/diode modules used in this topology (12 versus 9).

The reactive power injections on buses N8 and N14 are shown in the top and middle plots of Fig. 6 respectively. The BTB topology injects reactive power into both nodes to increase the voltages thereby reducing the overall system losses. It can be observed that the reactive power of bus N8 is much higher than that of bus N14, especially around noon, because the transfer of active power from bus N8 to bus N14 causes a reduction of the voltages within feeder 1. The rest of the topologies performs completely different since the reactive power is injected in node 8 and absorbed in node 14. This means that the reactive power is transferred between these two nodes just in the opposite direction than the active power flow. This is mainly controlled by the series converter and, therefore, the participation of the shunt converter for providing reactive power to the system is quite reduced as can be seen in the bottom plot of Fig. 6. This reactive power support just happens at noon during the peak of PV generation. This reduced participation of the shunt converter is justified due to the larger power losses in case of injecting more reactive power which is penalized by the objective function. Therefore, if the power losses of the converters are considered, the reactive power capability is not as relevant as initially expected. For this reason, the UPFC-P0Q and ShSPFC AC link are quite promising topologies because their reduced rated power and, therefore, lower investment costs.

The evolution of voltages on bus N8 and bus N14 for each type of FL are represented using violin plots in the upper and lower graphs of Fig. 7. These types of plots represents the distribution of quantitative data across several levels of one variable. The voltage at bus N8 located at the end of feeder 1, exhibits large voltage variations because the large power

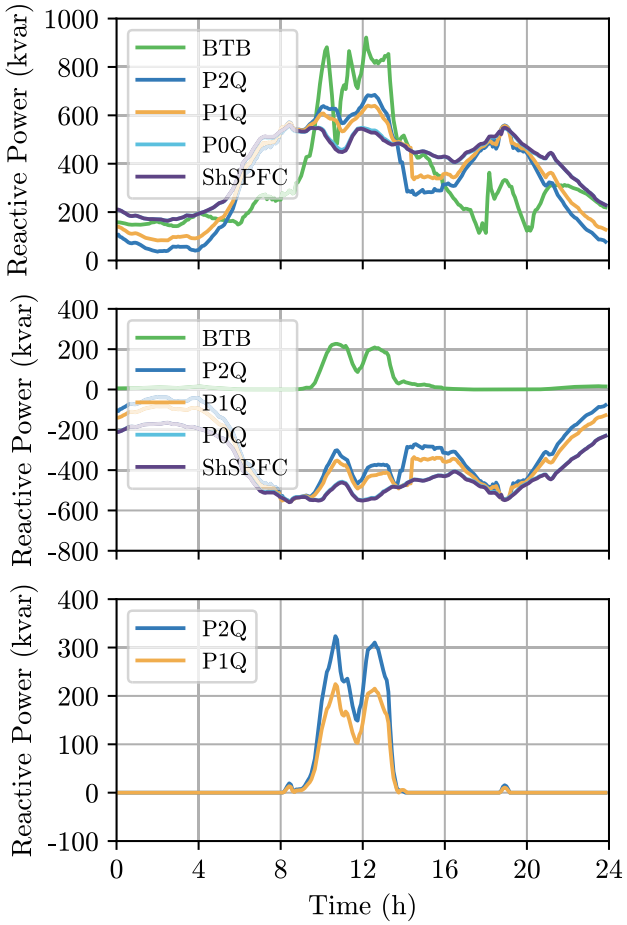

FIGURE 6. **Top plot: Reactive power injected to bus N8 by each FL. Medium plot: Reactive power injected to bus N14 by each FL. Bottom plot: Reactive power injection of VSCsh in the UPFC-P2Q and UPFC-P1Q topologies.**

injections of DERs. On the contrary, the voltage variations are quite reduce at node N14 located at the end of feeder 2 due to the absence of DERs. In the case of the BTB, it can be noticed that the voltage variation at N8 is reduced due to the active power transfer to the feeder 2 and, accordingly, the voltage at N14 increases. It is interesting to highlight that the voltages at nodes N8 and N14 are almost independent. In fact, the voltage variations at bus N8 are higher than those of N14. The main reason is that these nodes are connected through the DC link, which unbundles their corresponding voltages. Conversely, all the series topologies lead to similar voltage levels at nodes N8 and N14 since they are related through the injected series voltage. Moreover, the voltage variations in these node are much lower than in the previous cases. This is due to the fact that these topologies transfer almost twice active power than the BTB topology as shown in the bottom plot of Fig. 4.

The performance of FL topologies is completed with the computation of the previously defined KPIs and summarized in Table 2. The first and second rows correspond to the system energy losses, E_{Loss} in MWh, and their variation with respect

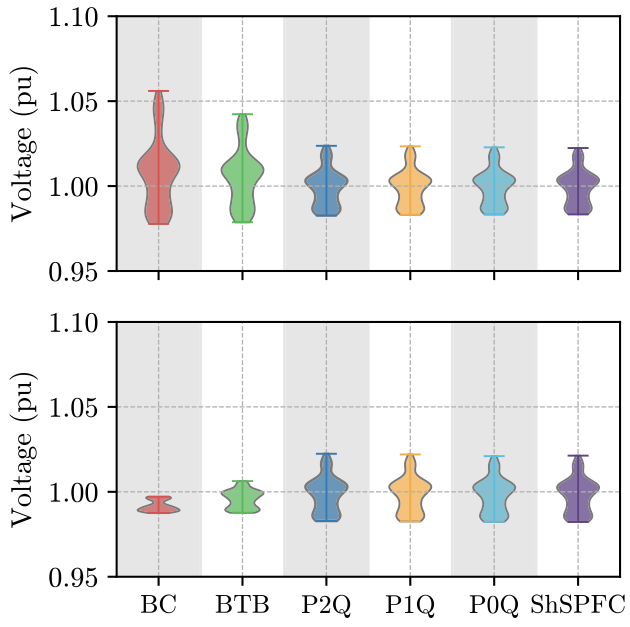

FIGURE 7. Top plot: Voltage of Node N8 for the case studies in violin format. Bottom plot: Voltage of Node N14 for the case studies in violin format.

to BC, ΔE_{Loss} (%). The FL topologies with series converter reduce the losses, with the ShSPFC topology being the best performer due to its reduced number of power electronic switches. On the contrary, the BTB topology leads to a power loss increase mainly due to the VSC power losses during off-peak PV periods.

The weight of each FL topology with respect the total system losses is measured by the KPI $R_{FL-syst}$ (%). Note that the higher values of this KPI correspond to the topologies with larger converters, BTB and UPFC-P2Q, which account for almost a 1/3 of the total system power losses. On the contrary, series FL topologies, specially those with converters with low rated power, UPFC-P0Q and ShSPFC AC link, have a relatively low impact on the total system losses.

The KPI relative to the reactive power R_Q evidences that the weight of the reactive power is relatively low with respect to the FL aparent power. The FL is mainly used for transferring active power between the interconnected feeders. Therefore, this KPI evidences that the use of topologies with reduced reactive power capability, i.e. UPFC-P0Q and ShSPFC AC link, could be interesting due to the lower rating of their power converters. The next KPI corresponds to the ratio between the maximum FL apparent power and the FL converter rated power, R_S (%). This ratio shows that BTB has the lowest R_S, close to 1, since it is a cascade topology. Note how this KPI almost doubles in the case of UPFC-P2Q due to the introduction of the shunt-series arrangement. Moreover, the increase of this KPI is dramatic if the shunt converter power rating is reduced, which indicates that this topology may force a power transfer between the feeders with a low-rated power converters.

TABLE 2. Values of the KPIs for the BC and different FL topologies.

KPIs (Units)	BC	BTB	P2Q	P1Q	P0Q	ShSPFC
E_{Loss} (MWh)	3.74	3.92	3.08	2.67	2.42	2.35
ΔE_{Loss} (%)	-	-4.65	17.85	28.58	35.47	37.37
$R_{FL-syst}$ (%)	-	34.38	31.34	20.78	11.97	9.25
$R_Q(\%)$	-	24.176	17.500	18.737	20.933	20.938
$R_S(\%)$	-	0.969	1.990	3.649	10.927	22.052
$V_{f1}(pu)$	1.0044	1.0028	0.9979	0.9980	0.9982	0.9982
$V_{f2}(pu)$	0.9918	0.9942	0.9952	0.9951	0.9948	0.9948

Finally, the KPIs V_{f1} and V_{f2} evaluate the daily average voltage of feeders 1 and 2 in per unit, respectively. All the topologies tend to reduce the average voltage in feeder 1 as a result of the active power transfer to feeder 2, thereby increasing the average voltage in feeder 2.

V. CONCLUSION

This paper has presented a comprehensive performance comparison of different FL topologies considering a detailed converter power loss model. Particularly, two types of FL topologies have been considered: DC links based on VSCs and AC links based on VeSCs. Within the DC-link group, the BTB and the UPFC topologies with different reactive power capability (namely P2Q, P1Q and P0Q) have been evaluated. From the AC-link side, the AC-link ShSPFC topology has been analyzed.

The power losses of each power converter, VSC or VeSC, have been formulated and parametrized using information provided by the manufacturer datasheets and detailed in the appendix of the paper. This detailed power loss model has been integrated into an OPF algorithm, which is responsible for calculating the optimal FL setpoints with the aim of reducing the total system power losses, taking into account the operational constraints of the FL and the distribution network.

The comparison of the different FL topologies has been done using the MV benchmark distribution network provided by the CIGRE Task Force C06.04.02 with a scenario of massive RES penetration. The simulation results have been complemented with the computation of a set of KPIs in order to present a fair and quantitative comparison of the performance of the different FL topologies.

The results have evidenced the importance of using a proper FL power loss model, as the impact of these losses can be relevant in the total system losses, particularly in the BTB topology due to its cascade nature. In this case, all power flows between the interconnected feeders pass through the VSCs, resulting in large power losses. On the contrary, the use of the alternative shunt-series DC or AC arrangements leads to a significant reduction in power losses. This reduction is

more remarkable in case of topologies with lower power converter ratings, i.e. UPFC-P0Q and AC-link ShSPFC. In this sense, the reactive power capability of the FL is not as relevant as initially expected if the objective function is to reduce the total system power losses. All topologies prefer to use their capacity to manage active power rather than reactive power to reduce power losses. In terms of voltage evolution, the management of active and reactive power flows by the FL tends to equalize the nodal voltages in the interconnected feeders and concentrate them around the nominal voltage.

In conclusion, the consideration of a detailed FL power loss model has revealed that shunt-series FL topologies can be an interesting option for reducing the power losses of distribution systems with limited investment, due to the low power rating of the converters required to transfer power between the interconnected feeders.

Future work could analyse other aspects of the use of FLs in distribution systems, such as their sizing and optimal placement in the grid, with the aim of selecting the most appropriate technology to enable massive RES integration.

APPENDIX
PARAMETERS OF THE IGBT/DIODE MODULE

This appendix collects the parameters of the IGBT/diode module SKM1000GB17R8 required to compute the FL power losses in Table 3.

TABLE 3. Typical parameters of the IGBT/diode module SKM1000GB17R8 at 150 °C.

Parameter	Magnitude	Parameter	Magnitude
r_{ce}	1.06 mΩ	v_{rr}	900 V
r_f	0.73 mΩ	i_{on}	1000 A
v_{ceo}	0.95 V	i_{off}	1000 A
v_{fo}	1.08 V	i_{rr}	1000 A
f_{sw}	3 kHz	E_{on}^{rat}	465 mJ
v_{on}	900 V	E_{off}^{rat}	332 mJ
v_{off}	900 V	E_{rr}^{rat}	159 mJ
p	3	q	60

The corresponding coefficients used in the fitting curve (16) are shown in Table 4.

TABLE 4. Coefficents of the switching power losses computed in mJ at 150 °C.

Coeff.	Magnitude	Param.	Magnitude	Param.	Magnitude
a_{on}	$5.238e^{-4}$	b_{on}	-0.26881	c_{on}	196.38095
a_{off}	$1.218e^{-5}$	b_{off}	0.22995	c_{off}	89.95238
a_{rr}	$-5.152e^{-5}$	b_{rr}	0.16855	c_{rr}	43.00000

REFERENCES

[1] International Energy Agency. (Apr. 21, 2020). *Global Energy Review 2021: Assessing the Effects of Economic Recoveries on Global Energy Demand and CO_2 Emissions in 2021*. R Package Version 1.0, Accessed: Mar. 12, 2022. [Online]. Available: https://www.iea.org/reports/global-energy-review-2021

[2] British Petroleum. *Statistical Review of World Energy 2022*. R Package Version 71st, Accessed: Mar. 12, 2022. [Online]. Available: https://www.bp.com/en/global/corporate/energy-economics/statistical-review-of-world-energy.html

[3] International Renewable Energy Agency. (Mar. 1, 2022). *World Energy Transitions Outlook: 1.5°C Pathway*. R Package Version 1.0, Accessed: Apr. 12, 2022. [Online]. Available: https://www.irena.org/publications/2022/mar/world-energy-transitions-outlook-2022

[4] E. Romero-Ramos, A. Gómez-Expósito, A. Marano-Marcolini, J. M. Maza-Ortega, and J. L. Martinez-Ramos, "Assessing the loadability of active distribution networks in the presence of DC controllable links," *IET Gener., Transmiss. Distrib.*, vol. 5, no. 11, pp. 1105–1113, Nov. 2011, doi: 10.1049/iet-gtd.2011.0080.

[5] W. Cao, J. Wu, N. Jenkins, C. Wang, and T. Green, "Benefits analysis of soft open points for electrical distribution network operation," *Appl. Energy*, vol. 165, pp. 36–47, Mar. 2016, doi: 10.1016/j.apenergy.2015.12.022.

[6] G. Venkataramanan, "Three-phase vector switching converters for power flow control," *IEE Proc. Electric Power Appl.*, vol. 151, no. 3, pp. 321–333, May 2004, doi: 10.1049/ip-epa:20040222.

[7] D. G. Holmes, "A unified modulation algorithm for voltage and current source inverters based on AC–AC matrix converter theory," *IEEE Trans. Ind. Appl.*, vol. 28, no. 1, pp. 31–40, Feb. 1992, doi: 10.1109/28.120210.

[8] Z. Yuan, Z. Du, C. Li, and T. An, "Dynamic equivalent model of VSC based on singular perturbation," *IET Gener., Transmiss. Distribution*, vol. 10, no. 14, pp. 3413–3422, Nov. 2016.

[9] M. Barragán-Villarejo, G. Venkataramanan, F. Mancilla-David, J. M. Maza-Ortega, and A. Gómez-Expósito, "Dynamic modelling and control of a shunt-series power flow controller based on AC-link," *Generation, Transmiss. Distribution*, vol. 6, no. 8, pp. 792–802, Aug. 2012.

[10] A. Nabavi-Niaki and M. R. Iravani, "Steady-state and dynamic models of unified power flow controller (UPFC) for power system studies," *IEEE Trans. Power Syst.*, vol. 11, no. 4, pp. 1937–1943, Dec. 1996, doi: 10.1109/59.544667.

[11] J. Beerten, S. Cole, and R. Belmans, "Generalized steady-state VSC MTDC model for sequential AC/DC power flow algorithms," *IEEE Trans. Power Syst.*, vol. 27, no. 2, pp. 821–829, May 2012, doi: 10.1109/TPWRS.2011.2177867.

[12] F. García-López, M. Barragán-Villarejo, A. Marano-Marcolini, J. Maza-Ortega, and J. Martínez-Ramos, "Experimental assessment of a centralised controller for high-RES active distribution networks," *Energies*, vol. 11, no. 12, p. 3364, Dec. 2018, doi: 10.3390/en11123364.

[13] T. W. May, Y. M. Yeap, and A. Ukil, "Comparative evaluation of power loss in HVAC and HVDC transmission systems," in *Proc. IEEE Region 10 Conf. (TENCON)*, Marina Bay Sands, Singapore, Nov. 2016, pp. 637–641.

[14] Y. Guo, H. Gao, Q. Wu, H. Zhao, and J. Østergaard, "Coordinated voltage control scheme for VSC-HVDC connected wind power plants," *IET Renew. Power Gener.*, vol. 12, no. 2, pp. 198–206, Feb. 2018.

[15] F. D. P. García-López, M. Barragán-Villarejo, J. M. Maza-Ortega, and A. Gómez-Expósito, "Multiterminal electrical charging station for LV networks," in *Proc. IEEE Eindhoven PowerTech*, Eindhoven, The Netherlands, Jun. 2015, pp. 1–5.

[16] M. Saeedian, B. Eskandari, S. Taheri, M. Hinkkanen, and E. Pouresmaeil, "A control technique based on distributed virtual inertia for high penetration of renewable energies under weak grid conditions," *IEEE Syst. J.*, vol. 15, no. 2, pp. 1825–1834, Jun. 2021, doi: 10.1109/JSYST.2020.2997392.

[17] G. Daelemans, K. Srivastava, M. Reza, S. Cole, and R. Belmans, "Minimization of steady-state losses in meshed networks using VSC HVDC," in *Proc. IEEE Power Energy Soc. Gen. Meeting*, Calgary, AB, Canada, Jul. 2009, pp. 1–5.

[18] Y. Zhang, X. Meng, A. M. Shotorbani, and L. Wang, "Minimization of AC-DC grid transmission loss and DC voltage deviation using adaptive droop control and improved AC-DC power flow algorithm," *IEEE Trans. Power Syst.*, vol. 36, no. 1, pp. 744–756, Jan. 2021, doi: 10.1109/TPWRS.2020.3020039.

[19] J. Ma, L. Yuan, Z. Zhao, and F. He, "Transmission loss optimization-based optimal power flow strategy by hierarchical control for DC microgrids," *IEEE Trans. Power Electron.*, vol. 32, no. 3, pp. 1952–1963, Mar. 2017, doi: 10.1109/TPEL.2016.2561301.

[20] Z. Yang, H. Zhong, A. Bose, Q. Xia, and C. Kang, "Optimal power flow in AC-DC grids with discrete control devices," *IEEE Trans. Power Syst.*, vol. 33, no. 2, pp. 1461–1472, Mar. 2018, doi: 10.1109/TPWRS.2017.2721971.
[21] Q. Nguyen, K.-W. Lao, P. Vu, and S. Santoso, "Loss minimization with optimal power dispatch in multi-frequency HVac power systems," *IEEE Trans. Power Syst.*, vol. 35, no. 3, pp. 1979–1989, May 2020, doi: 10.1109/TPWRS.2019.2953161.
[22] F. Mancilla-David, S. Bhattacharya, and G. Venkataramanan, "A comparative evaluation of series power-flow controllers using DC- and AC-link converters," *IEEE Trans. Power Del.*, vol. 23, no. 2, pp. 985–996, Apr. 2008, doi: 10.1109/TPWRD.2008.917702.
[23] C. Dhanamjayulu, P. Sanjeevikumar, and S. M. Muyeen, "A structural overview on transformer and transformer-less multi level inverters for renewable energy applications," *Energy Rep.*, vol. 8, pp. 10299–10333, Nov. 2022, doi: 10.1016/j.egyr.2022.07.166.
[24] F. Mancilla-David and G. Venkataramanan, "Realisation of an AC link unified power flow controller," *IET Gener., Transmiss. Distrib.*, vol. 6, no. 4, pp. 294–302, Apr. 2012.
[25] J. M. Maza-Ortega, M. Barragán-Villarejo, E. Romero-Ramos, A. Marano-Marcolini, and A. Gómez-Expósito, "Voltage source converter-based topologies to further integrate renewable energy sources in distribution systems," *IET Renew. Power Gener.*, vol. 6, no. 6, pp. 435–445, Nov. 2012, doi: 10.1049/iet-rpg.2011.0246.
[26] M. Barragán-Villarejo, A. Marano-Marcolini, J. M. Maza-Ortega, and A. Gómez-Expósito, "Steady-state model for the three-leg shunt-series AC-link power flow controller," *IET Gener., Transmiss. Distribution*, vol. 9, no. 16, pp. 2534–2543, Dec. 2015, doi: 10.1049/iet-gtd.2015.0068.
[27] D. Graovac and M. Pürschel. (Jan. 1, 2020). *IGBT Power Losses Calculation Using the Data-Sheet Parameters*. R Package Version 1.1. Accessed: Mar. 12, 2022. [Online]. Available: https://community.infineon.com/gfawx74859/attachments/gfawx74859/mosfetsisic/2197/2/IGBT_losscalculation.pdf
[28] K. Strunz, E. Abbasi, R. Fletcher, N. D. Hatziargyriou, R. Iravani, and G. Joos, "Benchmark systems for network integration of renewable and distributed energy resources," in *Proc. CIGRÉ*, Task Force C6.04.02, 1st ed. vol. 1, Apr. 2014, pp. 27–40.
[29] K. Rudion, A. Orths, Z. A. Styczynski, and K. Strunz, "Design of benchmark of medium voltage distribution network for investigation of DG integration," in *Proc. IEEE Power Eng. Soc. Gen. Meeting*, Montreal, QC, Canada, 2006, pp. 1–6.
[30] *Semikron Datasheet*, Skm1000Gb17R8, Semikron, Nuremberg, Germany, 2020. [Online]. Available: https://www.semikron-danfoss.com/products/product-classes/igbt-modules/detail/skm1000gb17r8-22898422.html
[31] A. S. Drud, "CONOPT: A system for large scale nonlinear optimization, reference manual for CONOPT subroutine library," ARKI, Consulting Develop. A/S, 69p, Bagsvaerd, Denmark, 1996.

FRANCISCO DE PAULA GARCÍA-LÓPEZ was born in Seville, Spain, in 1985. He received the electrical engineering, master's, and Ph.D. degrees from the University of Seville, Seville, in 2012, 2014, and 2018, respectively. Since 2012, he has been with the Department of Electrical Engineering, University of Seville, where he is currently an Assistant Professor. His research interests include power quality, control of power electronic devices, and integration of DERs.

MANUEL BARRAGÁN-VILLAREJO was born in Marmolejo, Spain, in 1984. He received the degree and Ph.D. degrees in electrical engineering from the University of Seville, Seville, Spain, in 2008 and 2014, respectively. Since 2008, he has been with the Department of Electrical Engineering, University of Seville, where he is currently an Associate Professor. His research interests include exploitation and control of power converter for smart grid management and grid integration of renewable energy resources.

ALEJANDRO MARANO-MARCOLINI (Member, IEEE) received the electrical engineering degree from the University of Malaga and the Ph.D. degree from the University of Seville, Spain, in 2010. He is currently an Associate Professor with the University of Seville. His research interests include voltage stability, integration of distributed generation, and optimization applied to power system engineering.

JOSÉ MARÍA MAZA-ORTEGA (Senior Member, IEEE) received the electrical engineering and Ph.D. degrees from the University of Seville, Seville, Spain, in 1996 and 2001, respectively. Since 1997, he has been with the Department of Electrical Engineering, University of Seville, where he is currently an Associate Professor. His research interests include power quality, harmonic filters, integration of renewable energies, and power electronics.